RSC Advances

PAPER

View Article Online
View Journal | View Issue

Cite this: *RSC Adv.*, 2024, **14**, 19096

Hydrothermally synthesized biofunctional ceria nanoparticles using orange peel extract: optimization, characterization, and antibacterial and antioxidant properties

Pegah Mohammadi,[a] Maliheh Yaghoobi,[b] Elnaz Keshavarz Bahaghighat[a] and Fatemeh Asjadi *[a]

In this research, cerium oxide nanoparticles were synthesized using orange peel extract *via* a hydrothermal method. An equal ratio of orange peel extract to cerium nitrate salt led to the formation of cerium hydroxide carbonate, whereas a 1 : 10 ratio formed cerium oxide. The hydrothermal treatment was conducted for durations of 5 and 25 hours. Scanning electron microscopy (SEM) images revealed that the hydrothermal samples treated for 5 hours exhibited significant agglomeration in both extract to salt ratios after heat treatment. X-ray diffraction patterns confirmed that all samples were converted into cerium oxide after heating at 500 °C for 3 hours. Based on XRD and SEM results, three cerium oxide samples, including those synthesized through the 25 hours hydrothermal process with a 1 : 10 ratio and the 25 hours hydrothermal process with both ratios and subsequent heat treatment, were selected for further investigation. Fourier transform infrared (FT-IR) analysis revealed more adsorption of the functional groups of orange peel extract on the surface of the as-synthesized sample. Moreover, the heat-treated sample with a 1 : 10 ratio, initially cerium oxide, displayed a higher amount of surface functional groups than the one with a 1 : 1 ratio which was initially cerium hydroxide carbonate. The antibacterial activities of the samples were determined using the colony count method. Activities of all samples against Gram-negative bacteria are in the range of 91.5–93.2% with a negligible difference, whereas the as-synthesized sample exhibited a superior activity of 96.6 ± 1.8% against Gram-positive bacteria compared to the other two heat-treated samples. The 87.3% antioxidant activity of the as-synthesized sample significantly surpassed that of the other two samples, as evaluated by the DPPH radical scavenging method.

Received 16th March 2024
Accepted 30th May 2024

DOI: 10.1039/d4ra02027h

rsc.li/rsc-advances

1. Introduction

In recent years, the synthesis of cerium oxide nanoparticles has gained considerable attention owing to their various applications. They possess a fluorite-type structure belonging to the *Fm*3*m* group.[1] CeO_2, or ceria, nanoparticles have been applied in biomedicine,[2,3] ultra-violet absorption,[4] sensors,[5] catalysts,[6,7] drug delivery systems,[8] antimicrobial ointments,[9] and environmental[10] fields on account of their desirable properties, namely high thermal stability,[11] redox properties,[11,12] high ionic conductivity,[12] oxygen storage ability,[11] ultra-violet absorption,[11,12] and antibacterial activities.[13]

The antimicrobial and antioxidant properties of cerium oxide have attracted significant attention in recent years. For instance, the high antibacterial efficiency of cerium oxide against five different pathogenic microorganisms, including *Escherichia coli*, *Salmonella typhimurium*, *Listeria monocytogenes*, *Staphylococcus aureus*, and *Bacillus cereus*, was reported.[13] Another investigation reported that 50 μg mL^{-1} is an optimum concentration of cerium oxide for antibacterial performance against different bacteria. A higher efficiency of antibacterial activity of CeO_2 nanoparticles was reported for *S. aureus*, *P. aeruginosa*, and *K. pneumoniae* than for *E. cloacae*, *E. faecium*, and *A. baumannii*.[14] Additionally, its antioxidant capacity has been reported in previous studies.[15] Cheng *et al.* reported its antioxidant properties using the DPPH radical-scavenging method.[16]

Cerium oxide nanoparticles have been synthesized through various methods, including co-precipitation,[17,18] sol–gel,[19,20] microwave combustion,[21] spray pyrolysis,[22] and hydrothermal methods.[23] The hydrothermal method is a simple technique that makes it possible to control the size and morphology of particles.

Recently, the utilization of plant extracts has received attention as an environmentally friendly method in nanoparticle synthesis[24,25] due to their abundance, natural safety,

[a]*Department of Materials Science and Engineering, Faculty of Engineering, University of Zanjan, P.O. Box 45371-38791, Zanjan, Iran. E-mail: Asjodi@znu.ac.ir*
[b]*Department of Chemical Engineering, Faculty of Engineering, University of Zanjan, P.O. Box 45371-38791, Zanjan, Iran*

and reliable source of reducing and stabilizing agents. Various plant extracts have been used for the synthesis of ceria nanoparticles, including *Melia dubia* leaves,[26] *Artabotrys hexapetalus* leaf,[27] *Salvia* seeds,[28] *Agathosma betulina*,[29] *Manilkara zapota* fruit peel,[30] *Aloe vera* leaves,[31] hemp leaves,[32] and tea waste.[10] However, achieving high crystallinity is a challenge in the plant extract-mediated synthesis of nanoparticles. Therefore, the green synthesized nanoparticles are subjected to heat treatment to overcome this issue in most cases. Various times and temperatures of heat treatment have employed for ceria nanoparticles. Ceria nanoparticles, with high antibacterial and photocatalytic properties, were synthesized using *Manilkara zapota* peel extract following heat treatment at 327 °C for 4 hours.[30] Salvia seed extract mediated synthesized ceria was heat treated at 400 °C for 2 hours.[28] Two hours of heat treatment at 600 °C were reported for ceria nanoparticles synthesized using *Moringa oleifera* leaf extract.[4]

This study emphasizes the synthesis, characterization, and comparative properties of cerium oxide nanoparticles and investigates the influence of synthesis conditions and heat treatment on their properties. Our research team responds to the mentioned challenges by combining hydrothermal and plant-mediated synthesis methods.[33,34] The results yielded improvements in crystallinity. Moreover, unlike the heat treatment stage, the hydrothermal process preserves functional groups from the plant extract on the nanoparticle surface. This study aims to examine the products synthesized by a hydrothermal method in the presence of orange peel extract with two different ratios of extract to salt. To the best of our knowledge, there has been no study on the green hydrothermal synthesis of ceria. In addition, the effect of the heat treatment process on the properties of ceria nanoparticles was investigated. The optimal sample was determined based on its antibacterial and antioxidant properties.

2. Experimental

2.1. Extraction of orange peel extract

To prepare the extract, orange peels harvested from gardens of Mazandaran province were utilized. Initially, the orange peels were dried at room temperature and powdered using an electrical mill. The powdered orange peels were mixed with distilled water in a 1 : 10 weight ratio and heated at 70 °C for 90 minutes. The mixture was filtered using filter paper and centrifuged at 3700 rpm after cooling. The prepared orange peel extract was used in the synthesis stage.

2.2. Synthesis of cerium oxide nanoparticles

A 0.5 M aqueous cerium nitrate salt solution was prepared. The orange peel extract was added dropwise to this solution. The pH was adjusted to 10 using a 2 M sodium hydroxide solution. The resulting solution was transferred into a Teflon-lined autoclave and heated to 150 °C for durations of 5 and 25 hours. The experiments were conducted with two extract ratios, 1 : 1 and 1 : 10. The product was collected by centrifugation, washed with water, and dried at room temperature. Part of the products were heat treated at 500 °C for 3 hours (with a heating rate of 5 °C min^{-1}). The naming scheme for the samples uses the extract to salt solution ratio, duration of hydrothermal process, and HT for heat-treated sample format. For instance, 1 : 1-5 h-HT is the sample synthesized with a 1 : 1 ratio of orange peel extract to cerium salt solution with a 5 hours hydrothermal process duration and heat treated for 3 hours at 500 °C.

2.3. Identification of synthesized nanoparticles

Nanoparticles were identified using X-ray diffraction (XRD) with a Panalytical X'PerPro diffractometer employing copper Kα radiation in the 2θ range of 10–90° with a step size of 0.05 and a time step of 1 second at room temperature. The particle morphology was examined using a scanning electron microscope (Mira3 Tescan). The peak characteristics of the XRD pattern were determined using Fityc software[35] and the Voight function. The FTIR spectra were obtained using a PerkinElmer Spectrum 400 spectrometer. N_2 adsorption and desorption cycles utilizing a BEISorp mini-II (Japan) were used for surface area, pore volume, and pore size. The transmission electron microscopy (TEM) analysis was performed using an EM 208s, and the nanoparticles' size distribution was determined using Image J software.[36]

The pH drift method was implemented to determine the pH_{pzc} of three selected samples. In brief, the initial pH of 20 mL of 0.05 M NaCl solution was adjusted between 2 and 12 using 0.1 M HCl and NaOH. 0.1 g of nanoparticles were added to each solution and kept on the shaker incubator for 24 h at 25 °C. The change in pH was recorded after 24 h. The pH_{PZC} point is a pH that is not changed after 24 hours.

2.4. Investigation of antibacterial activities of synthesized nanoparticles

The antibacterial activities of the synthesized ceria nanoparticles were evaluated by the colony count method. The bacteria used in this study were *Escherichia coli* and *Staphylococcus aureus* (ATCC 9637 and ATCC 12600) as representatives of Gram-negative and Gram-positive, respectively. All tools and nanoparticles were sterilized using an autoclave before the experiment. The entire procedure was carried out under a biological hood. First, a bacterial suspension was prepared, and its absorbance was read at a wavelength of 625 nm after vortexing and adjusted to 0.09 at 6×10^5 CFUs mL^{-1}. Then, 300 µl of the bacterial suspension was poured into sterilized microtubes containing 50 mg nanoparticles. The samples were incubated for 24 hours at 38 °C and then diluted at a 1 : 9 ratio with physiological saline. 10 µl of the diluted solution was spread on as-prepared agar Petri dishes. The plates were incubated for 24 hours at 37 °C. The antibacterial performance of the samples was evaluated the by colony counting method[37] to determine the number of viable bacteria. The bacteria removal was calculated using eqn (1), where R represents the percentage reduction, N_c is the number of colonies in the control Petri dishes, and N_s is the number of colonies in the samples.

$$R = \frac{N_c - N_s}{N_c} \quad (1)$$

Five Petri dishes were used as controls and samples of every bacterium and the average results were reported. All tests were repeated three times.

2.5. Antioxidant test

The DPPH (2,2-diphenyl-1-picrylhydrazyl) radical scavenging technique[38] was implemented for the antioxidant test. Four milliliters of DPPH solution with two concentrations of 40 mg L^{-1} in methanol were exposed to nanoparticles and incubated in darkness for 30 minutes.

The ceria nanoparticles were separated after 30 minutes using the 15 000 rpm centrifuge. The experiment was conducted using 12.5 and 7.5 mg mL^{-1} of nanoparticles. Subsequently, the absorbance of the supernatants was measured at the wavelength of 517 nm using a UV-vis spectrophotometer (BEL Engineering model UV-M51). As a result, the capabilities of different samples to quench the free radicals of the DPPH solution were determined. The reduction of absorbance was a criterion of antioxidant capacity. A greater reduction reveals higher antioxidant capacity. The inhibition percentage of ceria nanoparticles was calculated using the following relation.

$$\%\ \text{inhibition} = \frac{\text{absorbance of control} - \text{absorbance of sample}}{\text{absorbance of control}} \times 100 \quad (2)$$

3. Results and discussion

3.1. Phase and morphology characterization

Fig. 1 exhibits the XRD patterns of the as-synthesized samples. The amorphous product with no distinct characteristic peaks was formed after 5 hours of hydrothermal treatment in the same ratio of orange peel extract to cerium salt. Increasing the hydrothermal duration by 25 hours led to a low crystallinity cerium hydroxide carbonate ($CeCO_3OH$, JCPDS No. 41-0013). Decreasing the ratio of orange extract to salt to 1 : 10 resulted in the formation of ceria (JCPDS card no. 34-0394). Increasing the hydrothermal duration increased the crystallinity of the product.

Aqueous orange peel extract is composed of various classes of phytochemicals, including tannins, terpenoids, saponins, and flavonoids.[39] Some of these reported compounds are neochlorogenic, chlorogenic, caffeic, and ferulic acids, narirutin, hesperidin, didymin, sinensetin, nobiletin, and dimethylnobiletin.[40] These compounds can act as capping agents and reductants in nanoparticle synthesis due to the presence of hydroxyl groups.[41–43]

The formation of cerium hydroxide carbonate ($CeCO_3OH$) in a 1 : 1 ratio of orange peel extract to cerium nitrate can be clarified, considering the degradation of the present compounds in orange peel extract in the hydrothermal vessel.

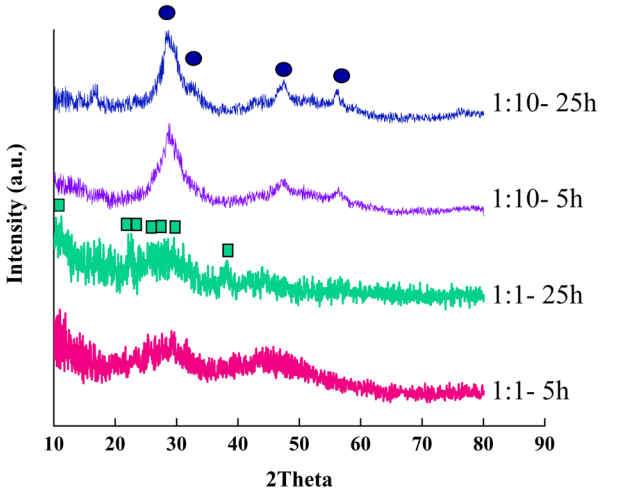

Fig. 1 XRD patterns of the as-synthesized samples with extract to cerium salt ratios of 1 : 10 and 1 : 1 and hydrothermal durations of 5 and 25 hours. ●: ceria; ■: cerium hydroxide carbonate.

There are compounds with C=O bonds in orange peel extract, namely caffeic acid, that can be dissociated to form carbonate ions. The decomposition of biocompounds of orange peel extract leads to liberating the carbonate ions in the reaction solution at high temperatures. The simultaneous presence of carbonate and metal oxide in the aqueous reaction medium leads to the formation of cerium hydroxide carbonate.

One possible path for the formation of the cerium hydroxide carbonate is the direct reaction of cerium nitrate with carbonate and OH ions.

$$Ce(NO_3)_3 \cdot 6H_2O + CO_3^{2-} + OH^- \rightarrow CeOHCO_3 + 6H_2O \quad (3)$$

However, the carbonate ions are not present in the solution to participate in reaction (3) before the dissociation of orange peel extract compounds in this study. Therefore, another mechanism, including the hydration and hydrolysis of Ce cations in solution, complex formation, and finally the precipitation of cerium hydroxide carbonate, is more likey in this case.[44]

$$[Ce(H_2O)_n]^{3+} + H_2O \leftrightarrow [Ce(OH)(H_2O)_{n-1}]^{2+} + H_3O^+ \quad (4)$$

$$[Ce(OH)(H_2O)_{n-1}]^{2+} + CO_3^{2-} \rightarrow CeOHCO_3 + (n-1)H_2O \quad (5)$$

$$H_3O^+ + OH^- \leftrightarrow 2H_2O \quad (6)$$

On the other hand, in the lower ratio of orange peel extract, the carbonate ions are in a lower concentration than in the high ratio, and, consequently, the dissolved carbonate ions are insufficient to change the reaction path and hence act mostly as a capping agent and reductant. The plant extract compounds attach to the surface of the particles and inhibit their growth. The compounds also can participate in reactions by supplying the OH ions in reactions. Cerium cations hydrolyse to form $[Ce(H_2O)_n]^{3+}$ in presence of NaOH. This intermediate turns to $Ce(OH)_3$, which also converts to CeO_2.[45] In addition, the

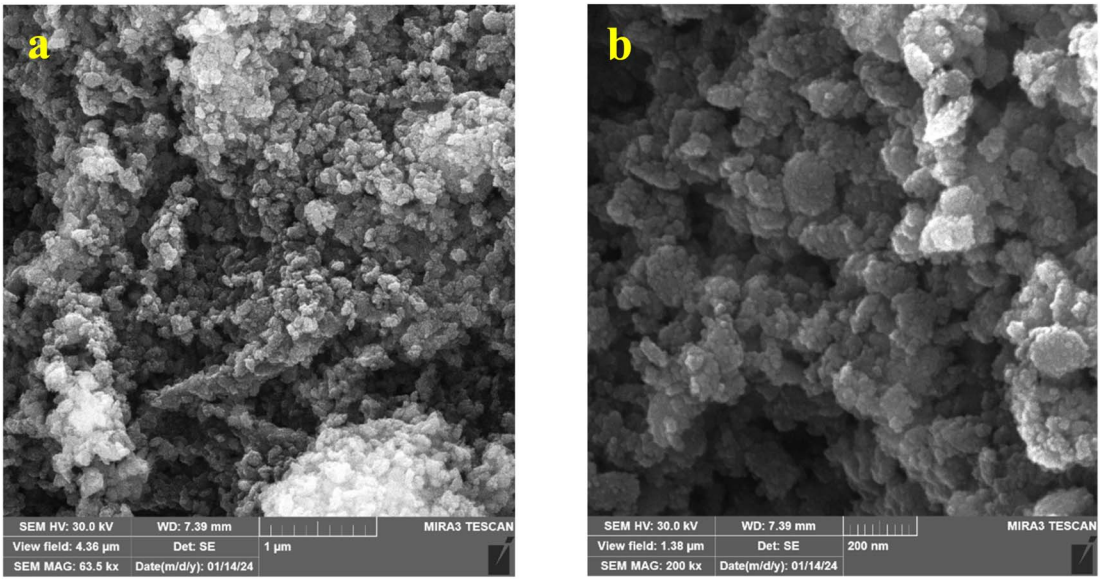

Fig. 2 SEM images of sample 1 : 10-25 h: (a) magnification of 30k× and (b) magnification of 200k×.

formation of a cerium complex in the presence of cerium nitrate and plant extracts has also been reported.[46] Therefore, the dissociation of these complexes to CeO_2 in the hydrothermal vessel is another possible mechanism for the formation of CeO_2 in a 1 : 10 ratio of orange peel extract to cerium salt.

Since sample 1 : 10-25 h was characterized as ceria and was more crystalized than sample 1 : 10-5 h, it was selected as the as-synthesized sample for the next investigations. The SEM images of this sample are shown in Fig. 2. The monodispersed homogeneous nanoparticles are evident in this image.

The TEM images of the sample and the nanoparticle size distribution are presented in Fig. 3. The results showed the spherical morphology of the nanoparticles. The average size of the nanoparticles was found to be 8.48 nm, with a standard deviation of 1.48 nm, indicating the narrow distribution of the nanoparticles.

All samples were heat treated at 500 °C for 3 hours to investigate the heat treatment effect. The XRD patterns of the heat-treated samples are presented in Fig. 4. All samples were pure well-crystallized ceria. No trace of hydroxide carbonate was detected in the patterns of the samples with the same ratio of extract to salt, implying its dissociation to form ceria.[47]

$$4CeOHCO_3 + O_2 \rightarrow 4CeO_2 + 4CO_2 + 2H_2O \quad (7)$$

The Williamson–Hall (W–H) formula was used to calculate the crystallite sizes of the three selected samples based on their XRD patterns. The formula presents the role of the lattice strain (ε) and crystallite size (D) in broadening the XRD peaks.[48]

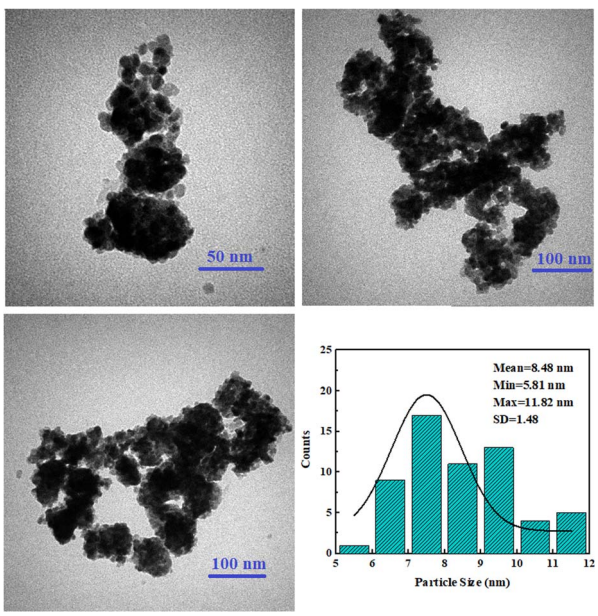

Fig. 3 TEM images and particle size distribution of the sample 1 : 10-25 h without heat treatment.

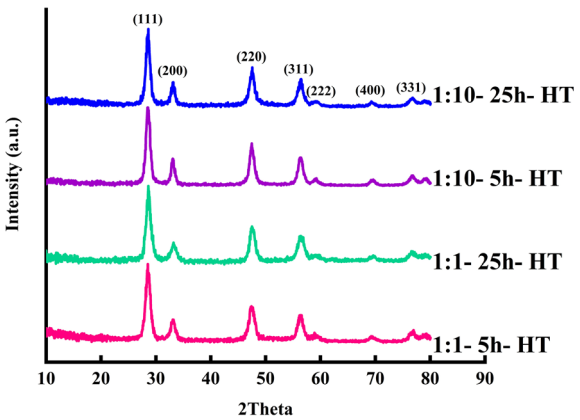

Fig. 4 XRD patterns of the samples after heat treatment at 500 °C for 3 hours.

$$\beta \cos\theta = K\lambda/D + 4\varepsilon \sin\theta \quad (8)$$

Here, λ is the incident wavelength, θ is the angle of diffraction and β is the FWHM of the peaks. The $\beta \cos\theta$–$4 \sin\theta$ graph is presented in Fig. 5. The higher slope and, consequently, higher lattice strain of the as-synthesized sample is evident in this figure. The higher strain can be attributed to oxygen vacancies and other stochiometric faults of the sample which are reduced drastically after calcination. The crystallite sizes were calculated based on the W–H equation, and the values are presented in Table 1. Though the crystallite size increases after calcination, the increment is not noticeable. The crystallite size of the as-synthesized sample is consistent with the TEM and SEM images and the size distribution of the particles implies the single crystal nature of the particles.

Fig. 6 shows the SEM images of the samples after heat treatment. The agglomeration of the nanoparticles with 5 h hydrothermal treatment compared to 25 h is clear in these images in both extract to salt ratios. The blue circles in Fig. 6a show a substantial degree of agglomeration. The agglomeration is probably due to less growth of particles and low crystallite sizes in 5 h of hydrothermal duration. Smaller particles possess more surface area and cause more agglomeration. Although the existence of an amorphous phase can be the reason for agglomeration, agglomeration did not occur in the 1 : 1-25 h-HT sample. As a result, the amorphous phase of the samples in this ratio, revealed in the XRD patterns, is not the reason for agglomeration. Due to these results, the 25 h hydrothermal treated samples for both extract to salt ratios were selected for further investigations. In brief, the synthesized sample 1 : 10-25 h and heat-treated samples 1 : 1-25 h-HT and 1 : 10-25 h-HT were selected for the rest of the analysis based on the XRD and SEM results.

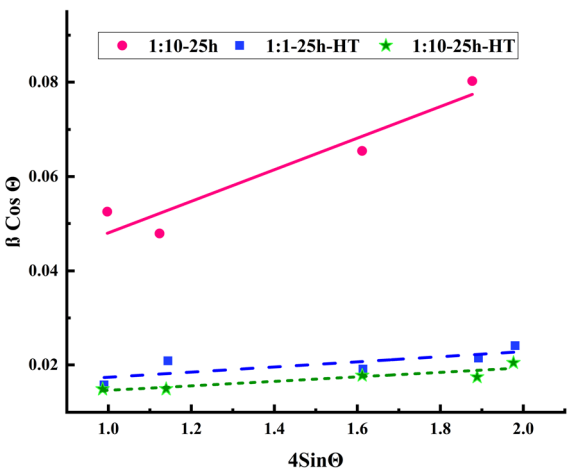

Fig. 5 $\beta \cos\theta$–$4 \sin\theta$ graph based on W–H equation for three selected samples.

Table 1 Crystallite size and lattice strain of samples calculated using the W–H equation

	Crystallite size (nm)	Lattice strain
1 : 10-25 h	10.7	0.033
1 : 10-25 h-HT	15.3	0.0048
1 : 1-25 h-HT	12.6	0.005

The BET results of these samples are tabulated in Table 2. The as-synthesized sample 1 : 10-25 h possesses a 6% larger surface area than the same heat-treated sample which is expected considering the effects of heat treatment on increasing the particle and crystallite sizes and the agglomeration of the particles. However, the 6% reduction of surface area after heat treatment is not significant. The surface area of sample 1 : 10-25 h-HT is approximately twice that of sample 1 : 1-25 h-HT. This could be for two reasons. First, there are the smaller particles of the sample with the same ratio of extract to salt. Since the extract molecules per product molecules are larger in this ratio, the biomolecules of extract provide a wider cover of formed nanoparticles, and the particles are smaller at the first stage. Smaller particles have a larger surface area and will cause more agglomeration in the heat treatment process. On the other hand, the conversion of carbonate to oxide occurred during the heat treatment of the sample with the same ratio. The different mechanisms of heat treatment could also be the reason for more agglomeration and lower surface area of this sample. This sample also possesses the lowest pore diameter.

The results of FTIR analysis for orange peel extract and three selected samples are depicted in Fig. 7. The FT-IR spectrum of the plant exhibits numerous peaks at various wavenumbers. The peaks observed at a wavenumber of 3420 cm^{-1} corresponds to the O–H stretching of the hydroxyl group.[20] The two peaks at 2860 and 2920 cm^{-1} are attributed to the symmetric and asymmetric stretching vibrations of the C–H bond.[20,49] The peak at 1613–1632 cm^{-1} is related to the N–H bond,[49] partially overlapping with the O–C–O and H–O–H peaks.[12] The band at ~1050 cm^{-1} represents the physical absorption of water.[50] The peak at the wavenumber of 1438 cm^{-1} originates from the carbonyl C=O, aromatic ring structure C=C, and ester C–O–C of polyphenols and flavonoids.[33] The peaks at 724 cm^{-1} and ~860 cm^{-1} are related to the bending modes of CO_2 (ref. 44) and CO_3^{2-}, respectively.[49] The numerous low intensity peaks at wavenumbers below 900 cm^{-1} represent the various compounds that are present in orange peel extract.

In the as-synthesized sample 1 : 10-25 h, some peaks match with those present in the plant extract. For instance, the stretching vibration of the C–H bond at 2920 and 2860 cm^{-1}. Two peaks in the range of 1539–1632 cm^{-1} are also similar to those in orange peel extract. Moreover, the uneven spectrum below 900 cm^{-1} confirms the presence of the extract compounds on the surface of this sample. In addition, a sharp peak around 1380 cm^{-1} in the as-synthesized sample, absent in the orange peel extract spectrum, corresponds to the nitrate group from the residual nitrate salt on the ceria surface.[51]

A reduction in the intensity of nitrate-related peaks is observed after heat treatment of the same sample, while peaks shared with the plant extract remain, indicating the presence of biocompounds of the extract on the surface of this sample. Furthermore, a new peak was observed at the wavenumber of

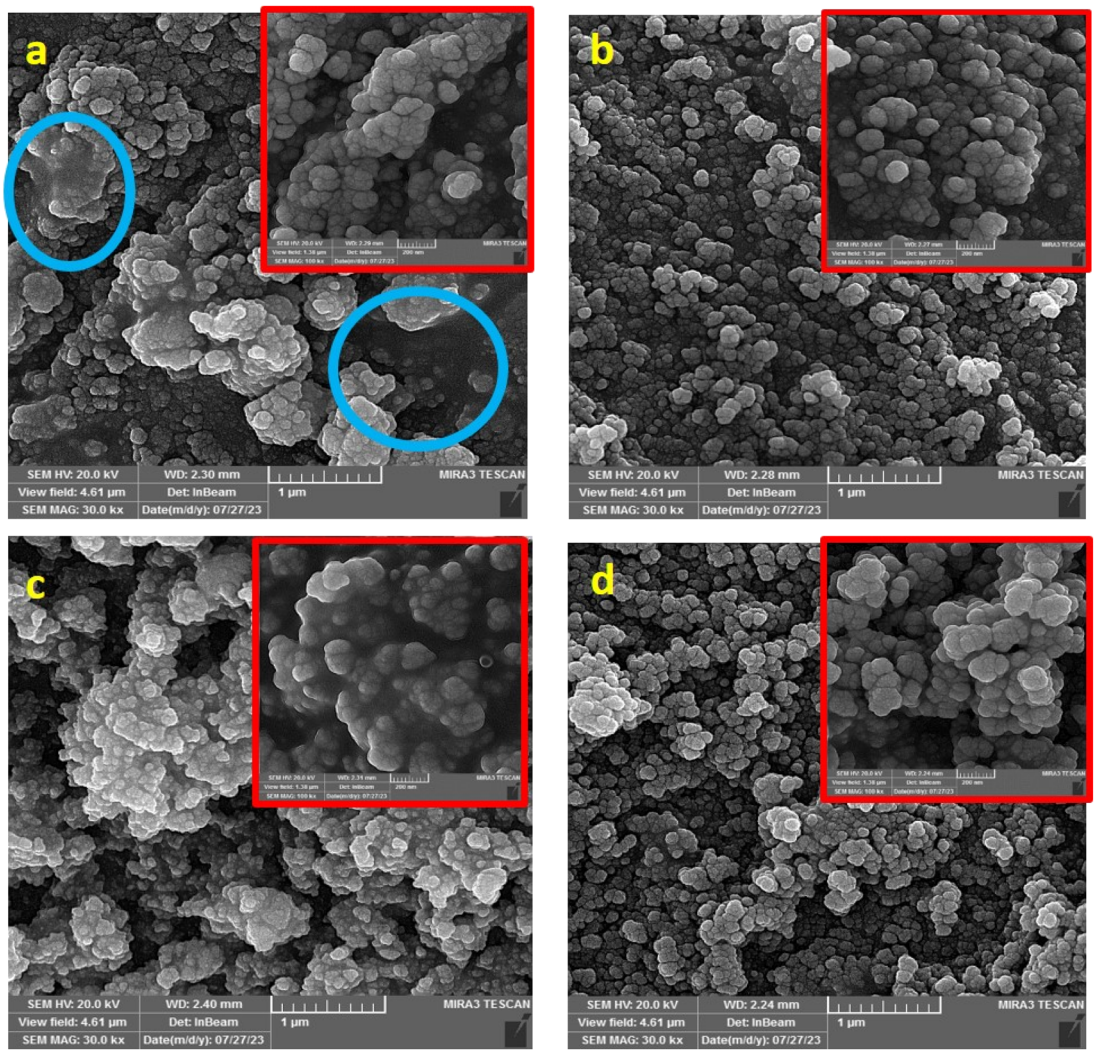

Fig. 6 SEM images of the samples heat-treated at 500 °C for 3 hours with different ratios of extract to salt: (a) 1 : 10 ratio, 5 h, (b) 1 : 10 ratio, 25 h, (c) 1 : 1 ratio, 5 h, (d) 1 : 1 ratio, 25 h.

Table 2 The BET results of the samples

Sample	BET surface area $m^2\ g^{-1}$	Pore volume $cm^3\ g^{-1}$	BJH pore diameter nm
1 : 10-25 h	79.26	0.28	2.7
1 : 10-25 h-HT	74.08	0.22	2.1
1 : 1-25 h-HT	36.49	0.28	1.9

550 cm^{-1}, corresponding to cerium oxide.[52,53] The peaks of CO_2 and CO_3^{2-} at 724 and 860 cm^{-1} still exist in this sample, while the spectrum is more even at wavenumbers lower than 900 cm^{-1}.

In the third sample, prepared with the same ratio of plant extract to salt and heat treated, 1 : 1-25 h-HT, the hydroxyl peaks are similar to those of the other samples. The extremely small peak of nitrate and N–H bond is still observable in this sample. However, most of the peaks shared with the plant extract have significantly dwindled. A new peak at wavenumber 503 cm^{-1} corresponds to the Ce–O bond.[44]

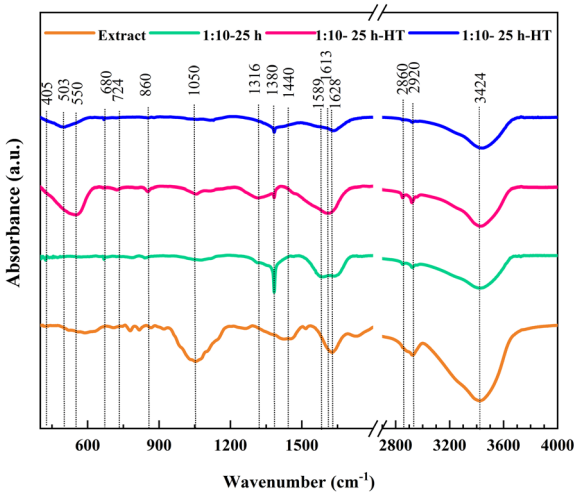

Fig. 7 FTIR spectra of the orange peel extract and samples 1 : 10-25 h, 1 : 10-25 h-HT, and 1 : 1-25 h-HT.

It is observed that the phytochemical compounds of the orange peel extract were adsorbed on the product surface, confirming their capping role in ceria synthesis. The as-synthesized sample exhibits the highest intensity for adsorbed functional groups, as was expected. Comparatively, the same sample after heat treatment possesses a smaller number of peaks with lower intensity, implying fewer adsorbed functional groups. However, the adsorbed groups in this sample are greater than those in the heat-treated sample prepared with a 1 : 1 ratio of orange peel extract to salt. At first glance, this may seem illogical, since the 1 : 1 ratio sample had a higher extract content and more contact with the functional groups. However, based on the X-ray diffraction results, different mechanisms led to the production of cerium oxide in these samples. In the sample synthesized with a 1 : 10 ratio of the extract, the hydrothermally produced powder has low crystallinity ceria, indicating the adsorption of functional groups on its surface. Therefore, no phase conversion occurred in the heat treatment process of this sample. In contrast, in the sample synthesized with a 1 : 1 ratio, different reactions occurred, as discussed before, and cerium hydroxide carbonate with low crystallinity was formed. The carbonate decomposes into cerium oxide during heat treatment. Consequently, the fewer adsorbed groups on the surface of this sample, resulting in the presence of fewer peaks in the FTIR spectrum, is understandable.

Considering the XRD, FTIR, and BET results, three cerium oxide samples were selected for antibacterial tests. The first, sample 1 : 10-25 h, exhibited very low crystallinity, high adsorbed groups from the plant extract, and a high specific surface area. The second sample, 1 : 10-25 h-HT, displayed high crystallinity, moderate surface adsorption factors, and an almost high specific surface area. The third sample, 1 : 1-25 h-HT, initially in carbonate form and transformed to cerium oxide during heat treatment, had the lowest specific surface area, high crystallinity, and low adsorbed surface functional groups compared to the other two samples.

3.2. Antibacterial and antioxidant tests

The antibacterial activities were assessed using the colony counting method. The removal percentages of the two bacteria, as well as the images of Petri dishes, are illustrated in Fig. 8a and b, respectively, after 24 hours of incubation at 37 °C.

All three CeO_2 samples have high antibacterial activity against both Gram-positive and Gram-negative bacteria. The minimum removal percentage is 84%. The activities of the three samples against *S.A.* bacteria are close to each other, and no sample was superior to the other samples. Regarding the *E.C.* bacteria, the as-synthesized sample shows higher activity than the other two. Heat treatment of the same sample decreases the antibacterial activity against *E.C.* bacteria. The lower removal percentage is for the sample 1 : 1-25 h-HT.

The higher specific surface area of the as-synthesized sample can increase its interaction with the bacterial cell membrane. Consequently, some of the bacteria's essential functions, such as cellular respiration, may alter. However, if the higher surface area plays a central role in the high antibacterial activity of the as-synthesized sample, this superiority should be observed in the killing of Gram-positive bacteria as well. There is not a significant difference in antibacterial activity among the three samples for Gram-positive bacteria. Therefore, this factor may not be the main reason explaining the observation.

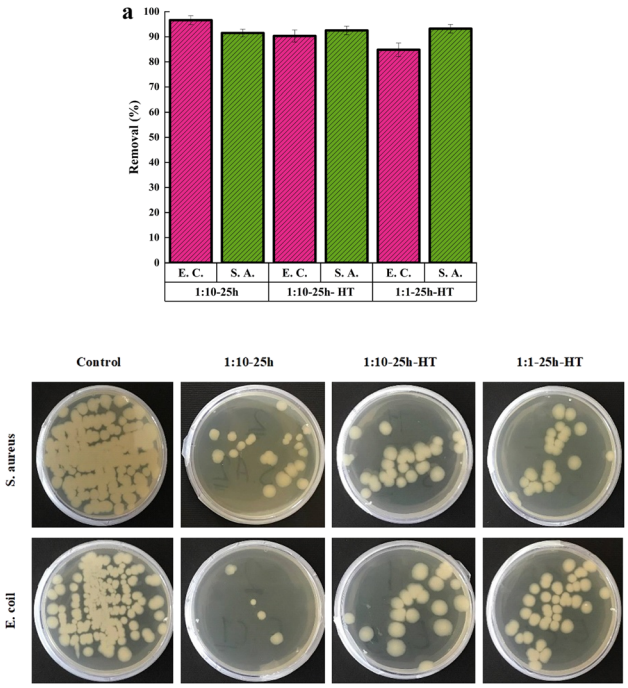

Fig. 8 (a) The removal percentages of *E.C.* and *S.A.* bacteria using three samples, (b) the images of Petri dishes after incubation at 37 °C for 24 h.

The electrostatic force is another factor that may affect the antibacterial effect. The pH_{PZC} was determined to investigate the effect of this factor. Fig. 9 demonstrates the results of the pH drift test to determine the pH_{PZC}. It shows that the pH_{PZC} are ~5.5, ~7.5, and ~8.5 for the as-synthesized sample and heat treated samples with 1 : 10 and 1 : 1 ratios of orange peel extract to cerium nitrate salt, respectively. It implies that the surface of the as-synthesized sample is more negative than those of the

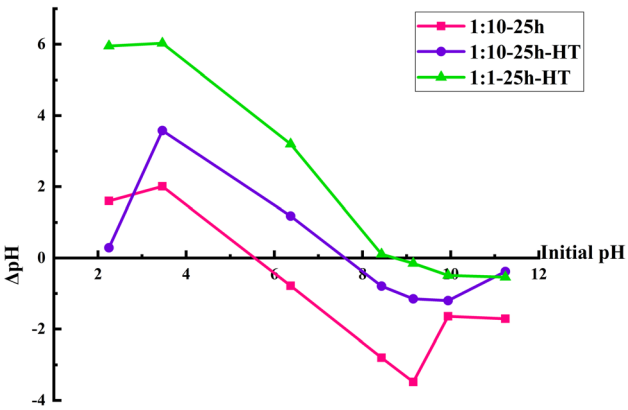

Fig. 9 ΔpH *versus* initial pH to determine pH_{PZC}.

other two samples. Considering these results and the fact that the bacterium's surface possesses a negative charge led to the conclusion that electrostatic force has an insignificant role in the antibacterial activity of the samples and other mechanisms are more prominent.

Another factor could be the higher number of surface functional groups in the as-synthesized sample, as previously confirmed by FTIR results. This factor can enhance electrostatic forces between bacteria and particles and potentially strengthen the antibacterial properties.

This justification has also been reported by other researchers.[54] The mutual electrostatic interaction of ions with positive charge with the negatively charged bacterial membrane and biomolecules (proteins and DNA) leads to structural changes and bacterial death. Therefore, the as-synthesized cerium oxide nanoparticles may exhibit a greater affinity for Gram-negative bacteria. Additionally, the FTIR results confirmed higher adsorption of surface factors on the heat-treated sample with an extract to salt ratio of 1 : 10 compared to that with the 1 : 1 ratio. Therefore, the sequence of antibacterial activity against *E.C.* bacteria is consistent with increasing order of adsorbed surface groups, based on FTIR results.

The precise mechanism of the antibacterial activity of cerium oxide nanoparticles is not clear. However, it is attributed to the generation of free radicals. Radicals produced by nanoparticles damage the bacterial cell membrane. Some researchers have reported that reactive oxygen species (ROS) naturally exist in intracellular and extracellular locations. Elevated ROS levels can increase oxidative stress within cells in some specific conditions. The cell membrane and internal cellular systems such as the respiratory apparatus would be harmed in these conditions. Under normal conditions, cells use antioxidant enzymes to defend against ROS-induced damage. However, nanoparticles that are present in cells can inhibit antioxidant enzymes to prevent the removal of ROS. As a result, the balance between the oxidation and antioxidant processes is disturbed by nanoparticles, leading to the accumulation of ROS inside the cell. Moreover, nanoparticles adhere to the cell membrane surface and induce instability in bacterial cellular respiration and permeability.[13,55]

The results of the antioxidant tests are depicted in Fig. 10. The as-synthesized sample exhibits significantly higher antioxidant activity compared to the other two samples. The as-synthesized 1 : 10-25 h sample has 6% more surface area than 1 : 10-25 h-HT. Therefore, the remarkable antioxidant performance of this sample cannot be due to higher surface area.

Since calcination causes Ce^{3+} to turn to ceria, in which Ce^{4+} is the prevalent type of cerium, there are more Ce^{3+} ions on the surface of the as-synthesized ceria compared to the heat-treated one. Fast oxidation of Ce^{3+} to Ce^{4+} by the existence of ROS led to the neutralization of ROS. This reaction is reversible. However, the reduction of Ce^{4+} to Ce^{3+} is slow. Hence, the higher Ce^{3+} on the surface of the as-synthesized sample imposes a higher antioxidant property on this sample. The other notable point is the role of plant extract compounds attached to the surface of the nanoparticles before calcination, which possess antioxidant properties. The antioxidants polyphenols present in orange peel

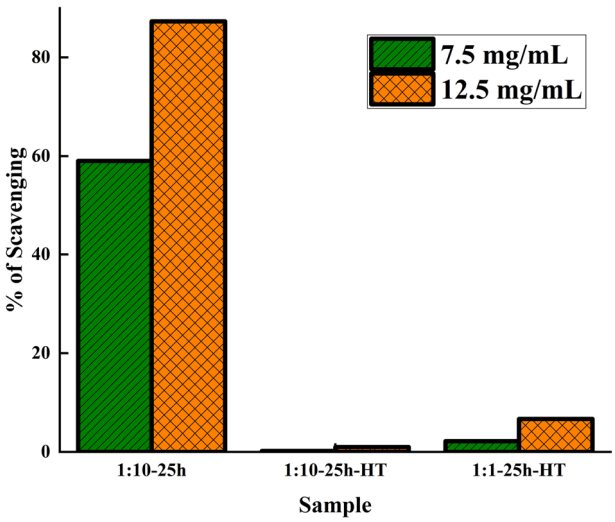

Fig. 10 DPPH radical scavenging activities of three samples at two nanoparticle concentrations of 12.5 and 7.5 mg mL^{-1}.

extract have been reported by other authors.[56] Heat treatment eliminated and degraded the adsorbed biomolecules and led to the consequent decrement of antioxidant activity.

The combination of Ce^{3+} and the polyphenol compounds' role makes the as-synthesized sample a greater antioxidant, while both factors diminish with heat treatment.

The experiments were repeated at higher nanoparticle concentrations, and the results were consistent with those of lower concentrations. The antioxidant performance of sample 1 : 1-25 h-HT was slightly better than that of 1 : 10-25 h-HT sample. Considering the lower surface area of this sample, these differences could be due to variations in the surface chemistry of the two samples. However, the efficiency of both heat-treated samples was extremely low. To the best of our knowledge, there is no report of such superiority of antioxidant ability in as-synthesized samples over heat-treated ones.

Considering the results of the antibacterial and antioxidant tests, it can be inferred that the as-synthesized sample prepared through the hydrothermal method has enormous potential for biomedical applications. These observations confirmed the central role of the adsorbed surface group in the biomedical properties of nanoparticles synthesized in the presence of plant extract.

4. Conclusions

Cerium oxide nanoparticles were synthesized using orange peel extract through the hydrothermal method. The ratio of extract to cerium salt was adjusted to be equal and 1 : 10. The former led to the formation of cerium hydroxide carbonate, while the latter caused the formation of cerium oxide. Increasing the hydrothermal duration increased the crystallinity of the products, but did not affect the type of the formed phases. All samples were converted to well-crystallized cerium oxide after heat treatment. The SEM images revealed the high agglomeration of the samples with a 5 hours hydrothermal treatment.

Further investigation was conducted on three less agglomerated cerium oxide samples: one with a 25 hours hydrothermal process and a 1 : 10 ratio without heat treatment, and two with a 25 hours hydrothermal process and ratios of 1 : 1 and 1 : 10 followed by heat treatment. The FTIR results confirmed more adsorption of functional groups on the as-synthesized sample. Among the heat-treated samples, the one with a 1 : 10 ratio, initially cerium oxide, possesses more adsorbed functional groups than the sample with a 1 : 1 ratio, initially cerium hydroxide carbonate. BET results showed the highest surface area, $\sim$79 $m^2\ g^{-1}$, for the as-synthesized sample. The surface area decreased after heat treatment of the same sample to $\sim$74 $m^2\ g^{-1}$. The minimum surface area, $\sim$36 $m^2\ g^{-1}$, was exhibited by the heat-treated sample with an extract to salt ratio of 1 : 1.

All three samples showed a high antibacterial performance. The antibacterial properties against Gram-negative bacteria were close in the three samples. However, the as-synthesized sample exhibited higher activity against *E.C.* bacteria. The superiority of the as-synthesized sample was disclosed in the antioxidant test. The antioxidant capacity of the as-synthesized sample was significantly larger than those of the other two samples due to more adsorbed functional groups on its surface.

Conflicts of interest

There are no conflicts to declare.

Acknowledgements

This work was supported by the University of Zanjan [Grant Agreement No. 1402-02].

References

1 V. Pathak, P. Lad, A. B. Thakkar, P. Thakor, M. P. Deshpande and S. Pandya, *Surface. Interfac.*, 2023, **11**, 100111.
2 K. Saravanakumar, A. Sathiyaseelan, A. V. A. Mariadoss and M.-H. Wang, *Ceram. Int.*, 2021, **47**, 8618–8626.
3 A. Zenerino, T. Boutard, C. Bignon, S. Amigoni, D. Josse, T. Devers and F. Guittard, *Toxicol Rep*, 2015, **2**, 1007–1013.
4 G. Eka Putri, Y. Rilda, S. Syukri, A. Labanni and S. Arief, *J. Mater. Res. Technol.*, 2021, **15**, 2355–2364.
5 H. Li, Y. Qu and X. Zhang, *Inorg. Chem. Commun.*, 2021, **130**, 108692.
6 M. Dubey, S. Wadhwa, A. Mathur and R. Kumar, *Appl. Surf. Sci. Adv.*, 2022, **12**, 100340.
7 P. Tamizhdurai, V. L. Mangesh, P. S. Krishnan, C. Kavitha, A. Vijay, R. Kumaran, M. Govindasamy, A. A. Alothman and M. Ouladsmane, *J. Saudi Chem. Soc.*, 2023, **27**, 101642.
8 X. Wu, Y. Zhang, Y. Lu, S. Pang, K. Yang, Z. Tian, Y. Pei, Y. Qu, F. Wang and Z. Pei, *J. Mater. Chem. B*, 2017, **5**, 3483–3487.
9 E. Barker, J. Shepherd and I. O. Asencio, *Molecules*, 2022, **27**, 2678.
10 C. Liu, X. Liu, Y. Wu, Z. Chen, Z. Wu, S. Wang, H. Han, Z. Xie, Y. Wang and T.-H. Ko, *Bioinorg. Chem. Appl.*, 2021, **2021**, 5285625.
11 M. Kurian, *J. Environ. Chem. Eng.*, 2020, **8**, 104439.
12 J. Calvache-Muñoz, F. A. Prado and J. E. Rodríguez-Páez, *Colloids Surf., A*, 2017, **529**, 146–159.
13 O. L. Pop, A. Mesaros, D. C. Vodnar, R. Suharoschi, F. Tăbăran, L. Mageruşan, I. S. Tódor, Z. Diaconeasa, A. Balint, L. Ciontea and C. Socaciu, *Nanomater.*, 2020, **10**, 1614.
14 M. A. Dar, R. Gul, P. Karuppiah, N. A. Al-Dhabi and A. A. Alfadda, *Crystals*, 2022, **12**, 179.
15 H. Nosrati, M. Heydari and M. Khodaei, *Mater. Today Bio*, 2023, **23**, 100823.
16 H. Cheng, Z. Shi, K. Yue, X. Huang, Y. Xu, C. Gao, Z. Yao, Y. S. Zhang and J. Wang, *Acta Biomater.*, 2021, **124**, 219–232.
17 D. Parimi, V. Sundararajan, O. Sadak, S. Gunasekaran, S. S. Mohideen and A. Sundaramurthy, *ACS Omega*, 2019, **4**, 104–113.
18 A. Rahdar, M. Aliahmad, M. Samani, M. HeidariMajd and M. A. B. H. Susan, *Ceram. Int.*, 2019, **45**, 7950–7955.
19 A. S. Fudala, W. M. Salih and F. F. Alkazaz, *Mater. Today: Proc.*, 2022, **49**, 2786–2792.
20 K. M. S. Khalil, L. A. Elkabee and B. Murphy, *Microporous Mesoporous Mater.*, 2005, **78**, 83–89.
21 P. Tamizhdurai, S. Sakthinathan, S.-M. Chen, K. Shanthi, S. Sivasanker and P. Sangeetha, *Sci. Rep.*, 2017, **7**, 46372.
22 Y. Wu, H. Li, X. Bian, W. Wu, Z. Wang and Y. Liu, *Materials*, 2021, **14**, 4963.
23 M. Lin, Z. Y. Fu, H. R. Tan, J. P. Y. Tan, S. C. Ng and E. Teo, *Cryst. Growth Des.*, 2012, **12**, 3296–3303.
24 A. Khan, N. Ahmad, H. Fazal, M. Ali, F. Akbar, I. Khan, M. Tayyab, M. N. Uddin, N. Ahmad, M. A. Abdel-Maksoud, I. A. Saleh, N. Zomot, H. AbdElgawad, K. Rauf, B. Iqbal, M. C. M. Teixeira Filho, M. A. El-Tayeb and A. Jalal, *RSC Adv.*, 2024, **14**, 5754–5763.
25 T. T. H. Le, T. T. Than, T. N. H. Lai and V. P. Le, *RSC Adv.*, 2024, **14**, 8779–8789.
26 N. J. Selvaraj Janaki, D. S. Ivan Jebakumar and P. Sumithraj Premkumar, *Mater. Today: Proc.*, 2022, **58**, 850–854.
27 S. Parvathy, G. Manjula, R. Balachandar and R. Subbaiya, *Mater. Lett.*, 2022, **314**, 131811.
28 P. Maleki, F. Nemati, A. Gholoobi, A. Hashemzadeh, Z. Sabouri and M. Darroudi, *Inorg. Chem. Commun.*, 2021, **131**, 108762.
29 F. T. Thema, D. Letsholathebe and K. Mphale, *Mater. Today: Proc.*, 2021, **36**, 435–439.
30 D. Ayodhya, A. Ambala, G. Balraj, M. Pradeep Kumar and P. Shyam, *Results Chem.*, 2022, **4**, 100441.
31 D. Dutta, R. Mukherjee, M. Patra, M. Banik, R. Dasgupta, M. Mukherjee and T. Basu, *Colloids Surf., B*, 2016, **147**, 45–53.
32 N. Korkmaz, D. Kısa, Y. Ceylan, E. Güçlü, F. Şen and A. Karadağ, *Inorg. Chem. Commun.*, 2024, **159**, 111797.
33 F. Asjadi and M. Yaghoobi, *Ceram. Int.*, 2022, **48**, 27027–27038.
34 M. Yaghoobi, F. Asjadi and M. Sanikhani, *J. Taiwan Inst. Chem. Eng.*, 2023, **144**, 104774.
35 M. Wojdyr, *J. Appl. Crystallogr.*, 2010, **43**, 1126–1128.

36 A. F. Stalder, G. Kulik, D. Sage, L. Barbieri and P. Hoffmann, *Colloids Surf., A*, 2006, **286**, 92–103.
37 N. Li, Z. Luo, C. Zeng, L. Chen, H. Yang and S. Gong, *SN Appl. Sci.*, 2019, **1**, 931.
38 S. Baliyan, R. Mukherjee, A. Priyadarshini, A. Vibhuti, A. Gupta, R. P. Pandey and C. M. Chang, *Molecules*, 2022, **27**, 1326.
39 S. Gotmare and J. Gade, *Int. J. ChemTech Res.*, 2018, **11**, 240–243.
40 M.-H. A. Oligie, L. O. Eduwuirofo, R. M. Iyekekpolor, O. Oghomwenrhiere, C. M. Ejimadu, E. I. Obasuyi, U. D. Archibong, O. T. Michael, R. O. Oghomwen and O. Iyekowa, *NIPES J. Sci. Technol. Res.*, 2023, **5**, 50–57.
41 D.-M. Radulescu, V.-A. Surdu, A. Ficai, D. Ficai, A.-M. Grumezescu and E. Andronescu, *Int. J. Mol. Sci.*, 2023, **24**, 15397.
42 U. O. Aigbe and O. A. Osibote, *J. Hazard. Mater. Adv.*, 2024, **13**, 100401.
43 A. Iqbal, A. S. Ahmed, N. Ahmad, A. Shafi, T. Ahamad, M. Z. Khan and S. Srivastava, *Environ. Nanotechnol., Monit. Manage.*, 2021, **16**, 100505.
44 H. S. Potdar, D.-W. Jeong, K.-S. Kim and H.-S. Roh, *Catal. Lett.*, 2011, **141**, 1268–1274.
45 H.-X. Mai, L.-D. Sun, Y.-W. Zhang, R. Si, W. Feng, H.-P. Zhang, H.-C. Liu and C.-H. Yan, *J. Phys. Chem. B*, 2005, **109**, 24380–24385.
46 M. Arshad, A. Iqbal, T. Ahamad, J. Gupta, M. Arshad and A. S. Ahmed, *J. Electron. Mater.*, 2023, **52**, 5690–5706.
47 F. Hrizi, H. Dhaouadi and F. Touati, *Ceram. Int.*, 2014, **40**, 25–30.
48 G. K. Williamson and W. H. Hall, *Acta Metall.*, 1953, **1**, 22–31.
49 F. Liu, L. Csetenyi and G. M. Gadd, *Appl. Microbiol. Biotechnol.*, 2019, **103**, 7217–7230.
50 S. W. Choi and J. Kim, *ACS Omega*, 2021, **6**, 26477–26488.
51 J. Seo, J. W. Lee, J. Moon, W. Sigmund and U. Paik, *ACS Appl. Mater. Interfaces*, 2014, **6**, 7388–7394.
52 M. E. Culica, A. L. Chibac-Scutaru, V. Melinte and S. Coseri, *Materials*, 2020, **13**, 2955.
53 A. Iqbal, T. Ahamad, F. A. Qais, N. Ahmad, A. Shafi, A. S. Ahmed and S. Srivastava, *Mater. Chem. Phys.*, 2023, **298**, 127397.
54 M. Nadeem, R. Khan, K. Afridi, A. Nadhman, S. Ullah, S. Faisal, Z. U. Mabood, C. Hano and B. H. Abbasi, *Int. J. Nanomed.*, 2020, **15**, 5951–5961.
55 S. Tavakoli, M. Kharaziha and S. Nemati, *Nano-Struct. Nano-Objects*, 2021, **25**, 100639.
56 D. Kalompatsios, V. Athanasiadis, D. Palaiogiannis, S. I. Lalas and D. P. Makris, *Beverages*, 2022, **8**, 71.